

Supporting Information for

**Spontaneous Aqueous Defluorination of Trifluoromethylphenols:
Substituent Effects and Revisiting the Mechanism**

Zhefei Guo^{1‡}, Geneviève W. Tremblay^{1‡}, Jingdan Chen², Shira Joudan^{1*}

[‡]Z.G. and G.W.T. contributed equally to this work

¹Department of Chemistry, University of Alberta, Edmonton, Alberta T6G 2G2, Canada

²Department of Chemistry, University of Illinois at Urbana-Champaign, Urbana, Illinois 61801, United States

E-mail: joudan@ualberta.ca

This supporting information contains 19 pages, including 5 tables and 11 figures.

SI-1. Chemicals

Ultrapure water (18.2 M Ω ·cm) was generated by Millipore EQ 7000 system. Sodium phosphate monobasic monohydrate (99.9%), sodium phosphate dibasic anhydrous (99.0%), sodium phosphate tribasic dodecahydrate (100.0%), sodium carbonate anhydrous (99.5%), 4-(trifluoromethyl)phenol (98%), 3-(trifluoromethyl)phenol (98+%), 2-(trifluoromethyl)phenol (99%), methanol (Optima Grade, 99.9%), phosphoric acid (85.0%), and TISAB II with CDTA were obtained from Fisher Scientific. Sodium bicarbonate (99.7%) was obtained from Caledon. 4-Hydroxybenzoic acid (99+%), 2-chloro-4-(trifluoromethyl)phenol (98%), and 3-chloro-4-hydroxybenzoic acid hemihydrate (98.0%) were obtained from TCI. 2-Hydroxybenzoic acid (99+%), 3-hydroxybenzoic acid (99%), hydrochloric acid (37%), and sodium fluoride were obtained from Sigma-Aldrich.

SI-2. Analytical Methods

Table S1. HPLC-UV method for quantifying trifluoromethylphenols (TFMPs) and corresponding TP hydroxybenzoic acids (HBAs).

Instrument	Waters Alliance 2695 HPLC coupled to a Waters 2487 Dual λ Absorbance Detector	
UV Detector	220 nm for 2-, 3-, and 4-TFMP. 226 nm for 2-Cl-4-TFMP.	
Wavelengths	The same wavelength was used for quantifying their corresponding HBAs.	
LC Parameters	Mobile Phase A	0.025% phosphoric acid in ultrapure water
	Mobile Phase B	HPLC grade methanol
	Column Temperature	30 °C
	Column	Poroshell 120 EC-C18, 50 \times 4.6 mm, 2.7 μ m
	Flow Rate	0.8 mL/min
	Injection Volume	20 μ L for 4-TFMP. 30 μ L for 2-TFMP, 3-TFMP, and 2-Cl-4-TFMP.
LC Gradient for 2-, 3-, and 4-TFMP	Time (min)	B
	0	20%
	0.2	20%
	1.5	60%
	4.0	60%
	4.01	20%
LC Gradient for 2-Cl-4-TFMP	Time (min)	B
	0	30%
	0.2	30%
	1.5	66%
	4.0	66%
	4.01	30%
9	30%	

Table S2. UHPLC-Orbitrap-HRMS method for transformation products analysis.

Instrument	Thermo Vanquish UHPLC coupled to a Thermo Scientific Exploris 240 Orbitrap	
MS Parameters	Ionization Mode	ESI Negative
	Ionization Voltage	2.4 kV
	Sheath Gas	50 Arb
	Aux Gas	10 Arb
	Sweep Gas	1 Arb
	Ion Transfer Tube Temperature	325 °C
	Vaporizer Temperature	350 °C
	Internal Mass Calibration	EASY-IC
Full Scan Acquisition Parameters	Scan Range (m/z)	50-750
	Orbitrap Resolution	120 000
	RF Lens (%)	70
	AGC Target	Standard
LC Parameters	Mobile Phase A	0.1% formic acid in ultrapure water
	Mobile Phase B	0.1% formic acid in methanol
	Column Temperature	40 °C
	Sample Temperature	7 °C
	Column	Luna Omega 1.6 µm Polar C18, 50 × 2.1 mm
	Flow Rate	0.35 mL/min
LC Gradient	Injection Volume	2 µL
	Time (min)	B
	-3.5 to -0.5 Pre-equilibration	5% at 0.6 mL/min
	-0.1 Pre-equilibration	5% at 0.35 mL/min
	0	5%
	0.5	5%
	6.5	75%
	7.5	98%
	9.5	98%
	11	5%

SI-3. *In situ* ¹⁹F NMR Experiment Details

The reaction mixture for the NMR data collection consisted of 1 mM 4-TFMP solution in a 5 mM carbonate buffer at pH 10.2. An aliquot of 630 µL of this solution was placed in an NMR tube and 70 µL of D₂O was added. Screening of the fluorinated species was conducted on an Agilent 400 MHz NMR (376 MHz for ¹⁹F NMR). The scan ranged from +70 to -70 ppm, in the hopes of capturing the benzoyl fluoride that was observed by UHPLC-Orbitrap-HRMS. The experiment consisted of an array NMR, where 128 scans were taken every 15 minutes, for a total of 12 spectra captured. The only products observed in the ranges detected were the initial 4-TFMP at -59.84, as well as an unexpected fluorinated product peak at -61.68 ppm. This is likely to be TP-4-3, as it is the result of a dimerization reaction that would preferentially occur at the higher tested concentrations.

benzoyl fluoride would be expected.

SI-4. DFT Calculation Details.

Implicit Solvation Model The Gibbs free energy (G_f) was derived by adding the thermo correction to free energy (G_f^{corr}) calculated at M06-2X/6-311+g(d,p)/IEFPCM level of theory and the electronic energy (EE) calculated at M06-2X/6-311++g(2d,2p) level of theory. For the Gibbs free energy of protons, the $G_{f, H^+, 1 \text{ atm}}$ used reported value of 6.3 kcal/mol.¹

To account for solvation, 1.89 kcal/mol was added as the correction for the standard state in solution (1 atm \rightarrow 1 M), and solvation free energy (ΔG_{solv}) was added (**eq S1**). ΔG_{solv} values for small polar inorganic molecules (H^+ , OH^- , F^- , H_2O , HF) were obtained from reported value: ΔG_{solv} for H^+ -265.9 kcal/mol, for OH^- -105.0 kcal/mol, for F^- -105.0 kcal/mol, for H_2O -6.3 kcal/mol, and for HF -7.6 kcal/mol.^{2,3} ΔG_{solv} values for organic molecules were obtained by subtracting the EE calculated in the gas state (EE_{gas}) from the EE calculated under the SMD model (EE_{smd}) at the M05-2X/6-31g(d) level of theory (**eq S2**).⁴ For reactions involving explicit H_2O , the G_f of H_2O was also corrected (+ 2.38 kcal/mol) for the concentration (55.3 M) difference from the concentration at the standard state (1 M) (**eq S3**).

$$G_f \text{ (kcal/mol)} = G_f^{\text{corr}} + EE + 1.89 + \Delta G_{\text{solv}} \quad \text{eq S1}$$

$$\Delta G_{\text{solv}} = EE_{\text{smd}} - EE_{\text{gas}} \quad \text{eq S2}$$

$$G_{f, H_2O} \text{ (kcal/mol)} = G_f^{\text{corr}, H_2O} + EE_{H_2O} + 1.89 + \Delta G_{\text{solv}, H_2O} + 2.38 \quad \text{eq S3}$$

Bond Dissociation Energy BDE of aryl- CF_3 C-F bond was calculated based on the enthalpy change of alkyl fluorine dissociation to two radical species in the gas phase. The enthalpy was calculated at the M06-2X/def2-TZVP level of theory based on the previously optimized structures. See **eq S4**.

$$\text{C-F BDE (kcal/mol)} = H_{\text{aryl-}CF_2\cdot} + H_{F\cdot} - H_{\text{aryl-}CF_3} \quad \text{eq S4}$$

Natural Population Analysis (NPA) Atomic charge analysis was done by natural population analysis⁵ using the same Gaussian 16 (Revision C.01) program at M06-2X/6-311+g(d,p)/IEFPCM level of theory.

SI-5. HBAs Phenol-OH Dissociation Equilibrium.

pKa values were from Advanced Chemistry Development (ACD/Labs) Software (© 1994-2024 ACD/Labs) unless otherwise indicated.

$$\%A^- = 100\% \times K_a / (K_a + [H]^+) \quad \text{eq S4}$$

$$\%HA = 100\% - \%A^- \quad \text{eq S5}$$

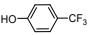
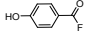
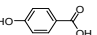
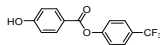
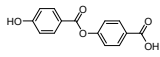
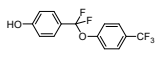
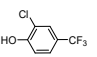
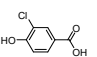
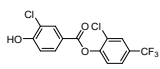
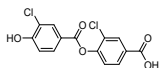
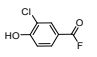
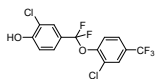
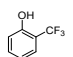
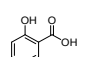
Table S3. Percent A⁻ and HA of 4-HBA, 2-HBA and 3-Cl-4-HBA at pH 6, pH 10 and pH 10.8. At all pH, the Ph-COOH was 100% deprotonated as A⁻ (Ph-COO⁻).

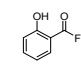
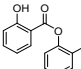
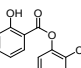
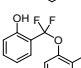
Compound	pKa of Ph-COOH	pKa of Ph-OH	pH (measured)	%A ⁻ (Ph-O ⁻)	%HA (Ph-OH)
4-HBA	4.25 ⁶	9.10 ⁶	10.81	98	2
			10.15	92	8
			6.18	0.1	>99
2-HBA	3.01 ⁷	13.6 ⁷	10.83	0	>99
			10.20	0	>99
			6.17	0	>99
3-Cl-4-HBA	4.25 ⁸	7.89 ⁸	10.78	>99	0
			10.16	>99	0
			6.18	2	98

SI-6. Suspect Screening for Transformation Products.

Chemical formulas of suspect intermediates and transformation products were hypothesized and their presences were confirmed by the full-scan MS chromatograms by extracting ions with a mass tolerance of 5 ppm (see instrument details in **Table S2**). The extracted chromatograms of qualified ions shall have Gaussian peak shapes.

Table S4. Suspect screening of 4-TFMP, 2-Cl-4-TFMP, and 2-TFMP hydrolysis transformation products. Compounds marked with an asterisk (*) indicate they have available standards. N.D. = not detected.

Compound	Structure	Ion formula [M-H] ⁻	Theoretical m/z, ESI ⁻	Observed m/z, ESI ⁻	Error (ppm)	RT (min)
4-TFMP*		C ₇ H ₄ F ₃ O ⁻	161.0220	161.0223	+1.86	6.37
TP-4-1		C ₇ H ₄ FO ₂ ⁻	139.0201	139.0204	+2.16	4.64
TP-4-2 (4-HBA)*		C ₇ H ₅ O ₃ ⁻	137.0244	137.0247	+2.19	3.52
TP-4-3		C ₁₄ H ₈ F ₃ O ₃ ⁻	281.0431	281.0438	+2.49	7.83
TP-4-4		C ₁₄ H ₉ O ₅ ⁻	257.0456	257.0449	-2.33	6.48
TP-4-5		C ₁₄ H ₈ F ₅ O ₂ ⁻	303.0450	N.D.	N.D.	N.D.
2-Cl-4-TFMP*		C ₇ H ₃ ClF ₃ O ⁻	194.9830	194.9830	-0.15	6.76
TP-2Cl-1 (3-Cl-4-HBA)*		C ₇ H ₄ ClO ₃ ⁻	170.9854	170.9855	+0.17	4.51
TP-2Cl-2		C ₁₄ H ₆ Cl ₂ F ₃ O ₃ ⁻	348.9652	348.9648	-1.07	8.12
TP-2Cl-3		C ₁₄ H ₇ Cl ₂ O ₅ ⁻	324.9676	324.9677	+0.34	7.42
TP-2Cl-4		C ₇ H ₄ ClFO ₂ ⁻	172.9811	N.D.	N.D.	N.D.
TP-2Cl-5		C ₁₄ H ₈ Cl ₂ F ₅ O ₂ ⁻	370.9671	N.D.	N.D.	N.D.
2-TFMP*		C ₇ H ₄ F ₃ O ⁻	161.0220	161.0221	+0.57	5.91
2-HBA (Salicylic)		C ₇ H ₅ O ₃ ⁻	137.0244	137.0245	+0.31	5.03

acid)*						
TP-2-1		$C_7H_4FO_2^-$	139.0201	N.D.	N.D.	N.D.
TP-2-2		$C_{14}H_8F_3O_3^-$	281.0431	N.D.	N.D.	N.D.
TP-2-3		$C_{14}H_9O_5^-$	257.0456	N.D.	N.D.	N.D.
TP-2-4		$C_{14}H_8F_5O_2^-$	303.0450	N.D.	N.D.	N.D.

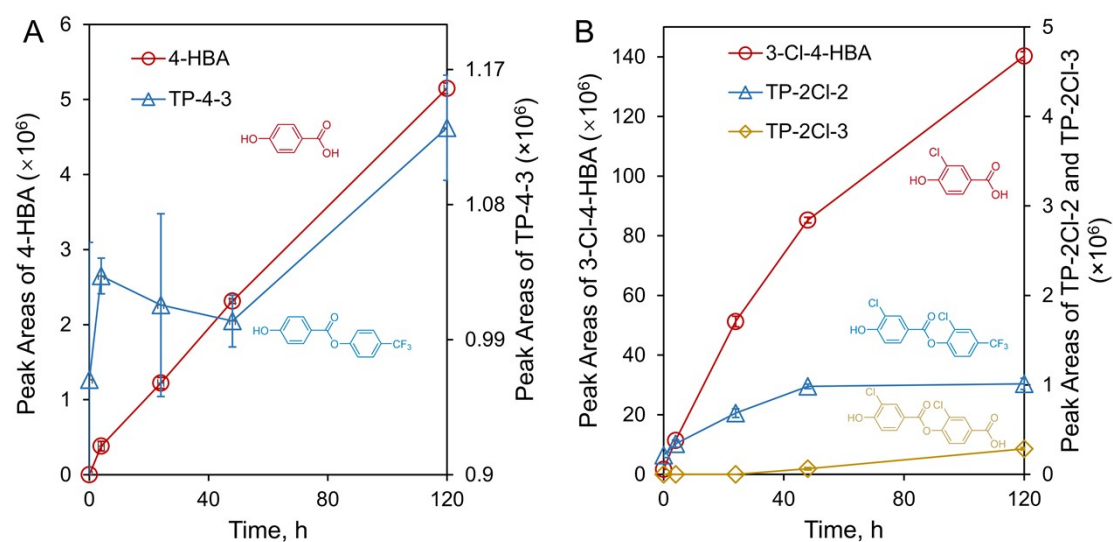


Figure S2. The plot of peak areas vs. time for transformation products from the aqueous hydrolysis defluorination of 4-TFMP (A) and 2-Cl-4-TFMP (B) at pH 6.2. Note that for TP-4-3, TP-2Cl-3, and TP-2Cl-3, the peak areas are plotted on the right y-axis.

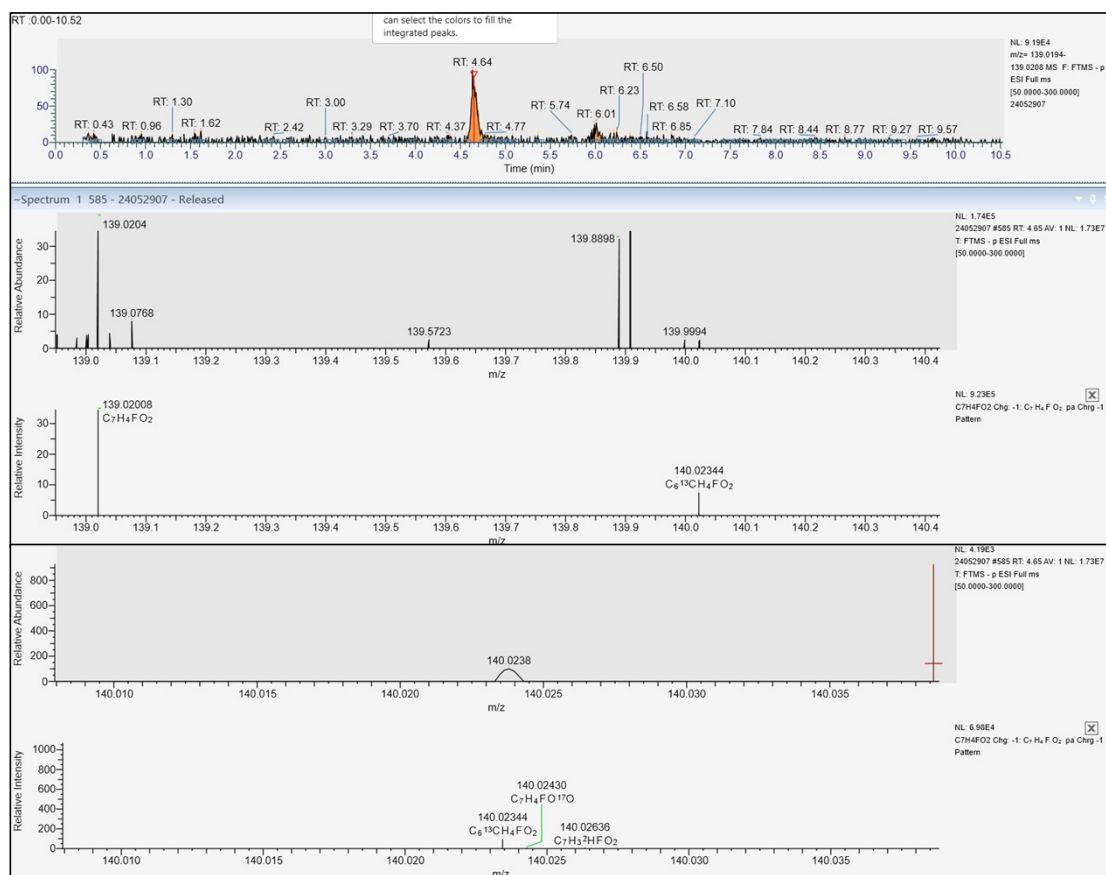


Figure S3. Identification of the benzoyl fluoride intermediate in the 4-TFMP hydrolysis at pH 10. The top panel shows the mass range extracted ion chromatogram. The middle panel shows a high-resolution mass spectrum of the sample, and the predicted isotope pattern of the proposed compound, $C_7H_4FO_2^-$. The bottom panel shows the high-resolution mass spectrum aligned with its second isotope, $C_6^{13}CH_4FO_2^-$.

SI-7. Stability of 3-TFMP towards Hydrolysis.

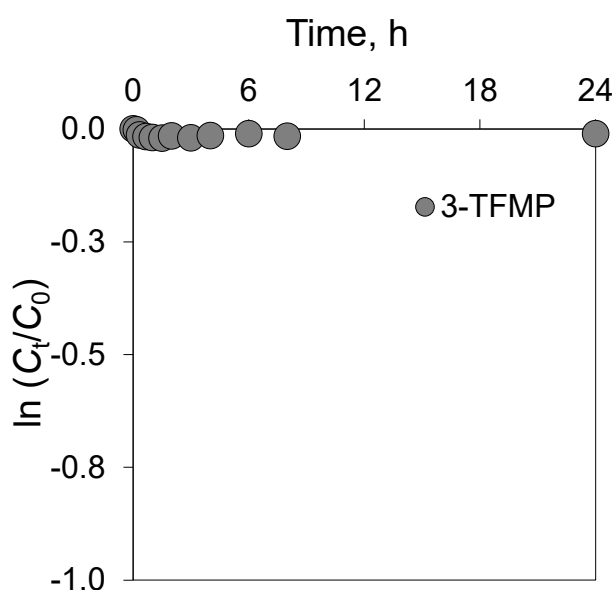
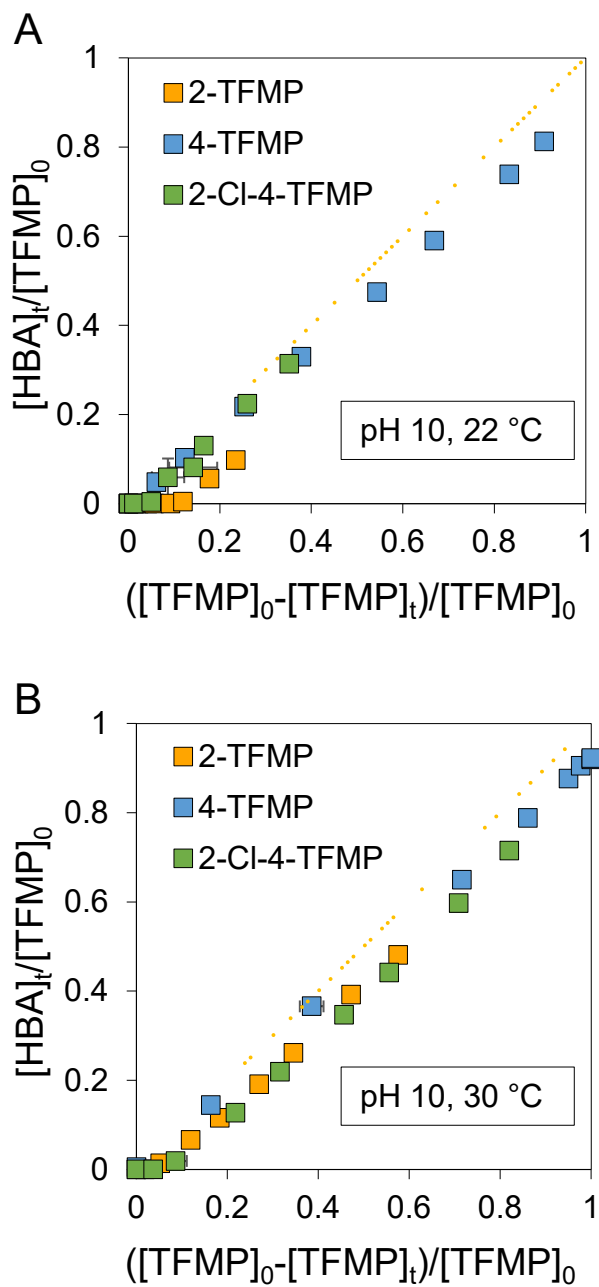


Figure S4. Stability of 3-TFMP over 24 hours in pH 10 carbonate buffer at 40 °C. Error bars are smaller than data points.

SI-8. Hydroxybenzoic Acid Formation.



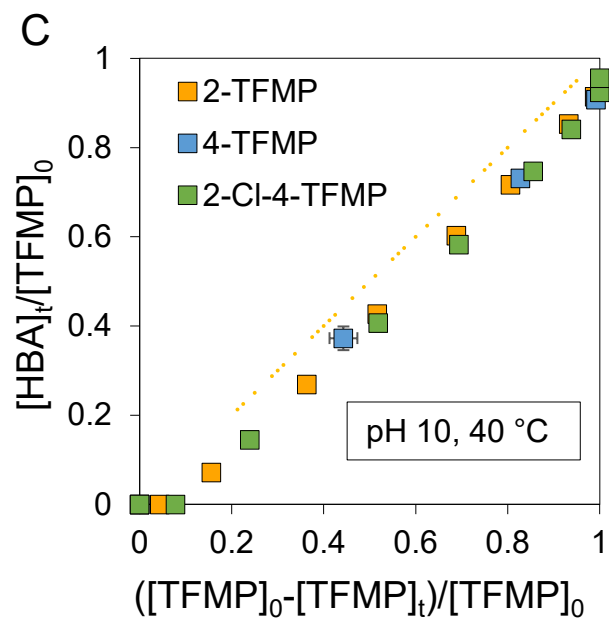
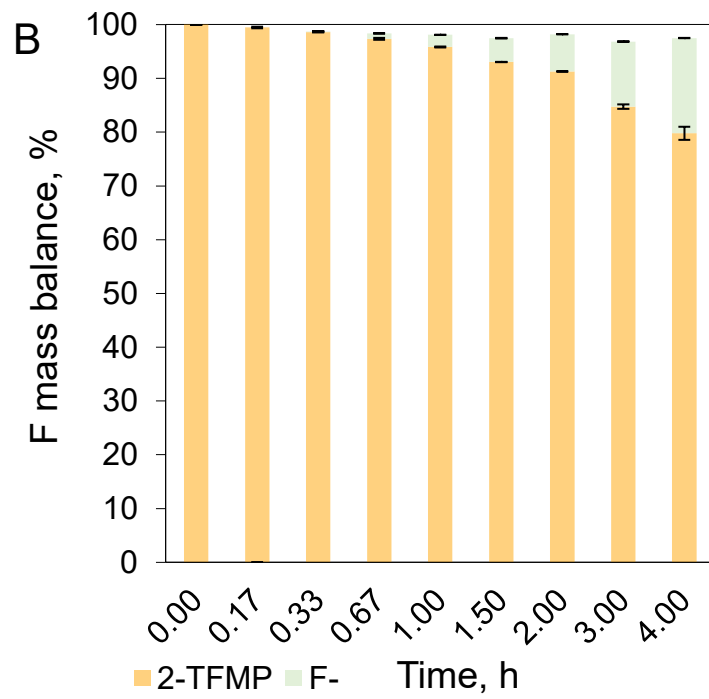
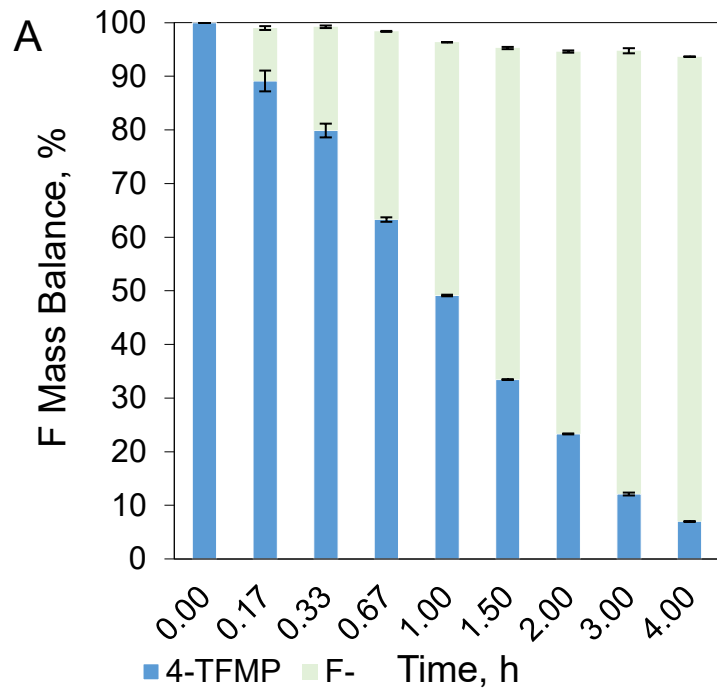


Figure S5. The plot of normalized HBA formation ($[HBA]_t/[TFMP]_0$) vs. normalized TFMP consumption ($([TFMP]_0 - [TFMP]_t)/[TFMP]_0$) under pH 10 at (A) 22 °C; (B) 30 °C; and (C) 40 °C. The yellow dashed line in (A), (B), and (C) indicates an ideal 1:1 stoichiometric relationship between TFMP consumption and HBA formation.

SI-9. Fluoride Mass Balance.



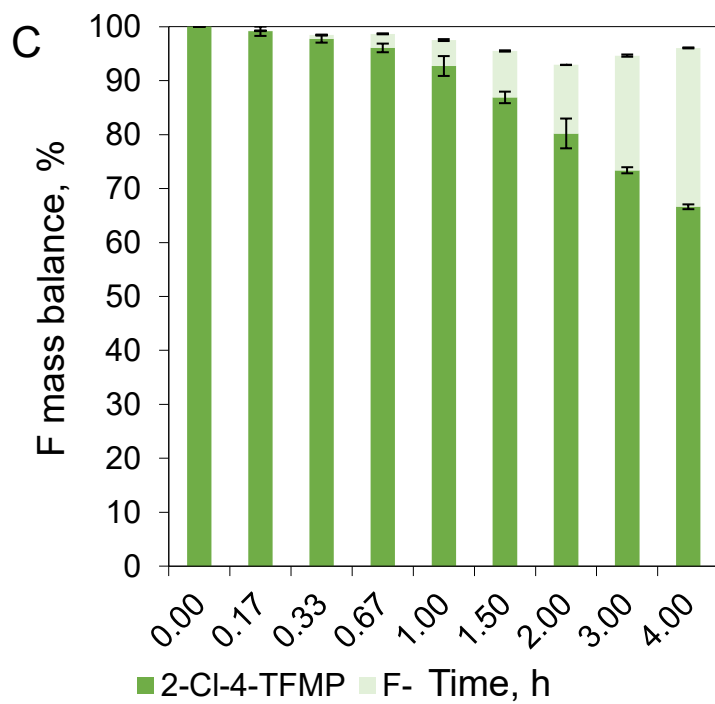


Figure S6. The fluoride mass balance over time of (A) 4-TFMP, (B) 2-TFMP, and (C) 2-Cl-4-TFMP.

SI-10. Schematic Diagram of the TFMP Hydrolysis Defluorination Including the Electron Pushing Arrows.

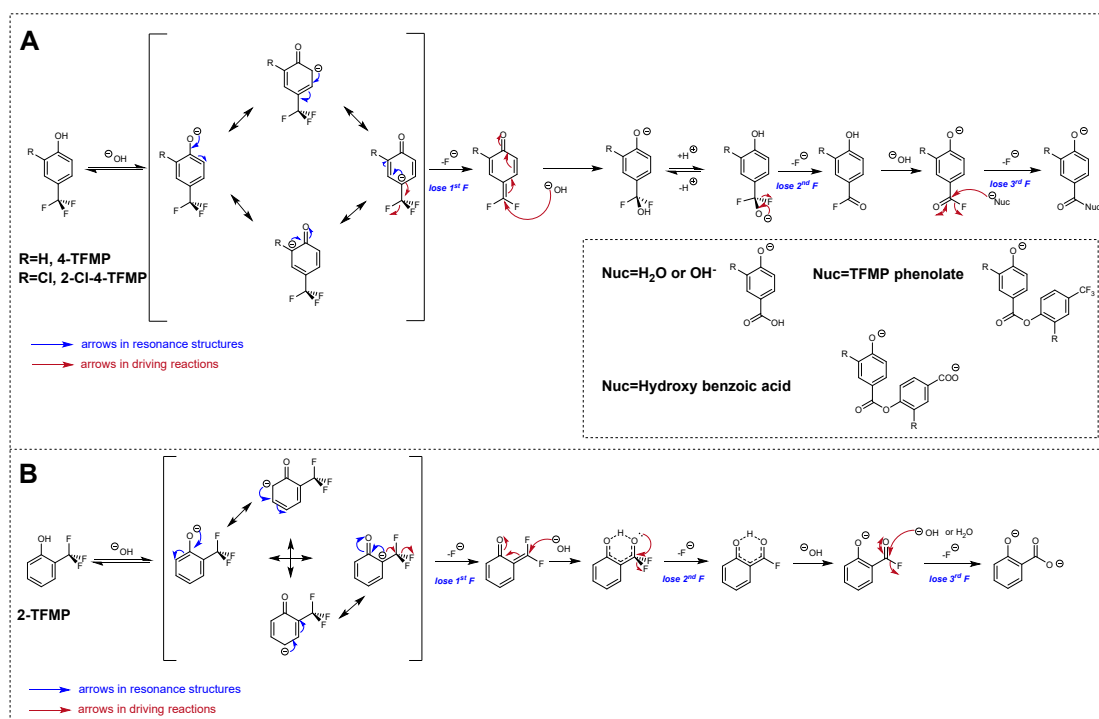


Figure S7. Detailed mechanism diagram of (A) 4-TFMP or 2-Cl-4-TFMP and (B) 2-TFMP aqueous defluorination including.

SI-11. Explicit Solvation for the Rate Determining Steps (the first steps) of TFMPs Spontaneous Defluorination in the Aqueous Phase.

Given the fact that the starting concentrations of TFMPs in the experiments were well below their solubility limits, significant hydration of charged and highly polarized intermediates is inevitable. This becomes particularly noteworthy when these hydrated intermediates are precursors to transition states in the rate-determining step (RDS). Thus, hybridized solvation model was used to properly account for the solvation effect during the RDS specifically. To properly account for explicit solvation effect in RDS, one, two, five, or six explicit water molecules participated scenarios are considered.

One or two explicit water molecules.

The addition of water molecules significantly stabilized the hydrophilic phenol-O⁻ group via hydrogen bonding (**Figure S9A** and **S9B**). For example, the ΔG of the reaction $[2\text{-TFMP}]^- + \text{H}_2\text{O} \rightarrow 2\text{-1Solv}$ was -3.1 kcal/mol (**Figure S9A**). However, explicit water molecules near the relatively hydrophobic $-\text{CF}_3$ group increased the energy. For instance, placing explicit waters near the $-\text{CF}_3$ of 4-TFMP and 2-Cl-4-TFMP increased their complex energies by 0.9 and 1.1 kcal/mol, respectively. This is attributed to the hydrophobic nature of the $-\text{CF}_3$ group, making hydration thermodynamically unfavorable at that site. When only one explicit water molecule was considered, the DFT-calculated ΔG^\ddagger values for the hydrolysis defluorination of 4-, 2-Cl-4-, and 2-TFMP were 25.8, 28.3, and 30.7 kcal/mol, respectively—substantially higher than the experimentally determined values of 22.6, 22.8, and 23.5 kcal/mol (**Figure S9A**). Adding two explicit water molecules did not significantly improve this overestimation (**Figure S9B**). To address this, five or six water molecules were tested.

Five or six explicit water molecules.

Considering the fact that solvation differs most at phenolate oxygen and $-\text{CF}_3$ group and limited by computational cost, five or six explicit waters were mainly placed around the two sites for geometry optimization and energy calculation in the corresponding structures. Strategy to decently generate water involved transition state and intermediate structures are elaborated as below in **Figure S8**. Firstly, Packmol⁹ was used for water solvated ball generation, in which 300 water molecules are placed in the sphere space with radius of 10 angstroms (\AA) centering target DFT optimized un-solvated molecule. Later, UFF force field¹⁰ was used for water relaxation. From relaxed solvation ball structure, thinner solvation layer (water molecules within 5 \AA) was preserved and further relaxed by using GFN-2(xtb).^{11,12} Finally, water molecules solvated around phenolate oxygen and $-\text{CF}_3$ group tightly with appropriate number as needed, were preserved for final DFT calculation. Throughout the semi-empirical and force field relaxation, central molecule was frozen all the way to preserve structure features at DFT level. DFT calculations reveal the hydrated intermediates in the RDS involve water molecules stabilizing the phenolate via hydrogen bonding, while the remaining water molecules form a hydrogen-bond network around the $-\text{CF}_3$.

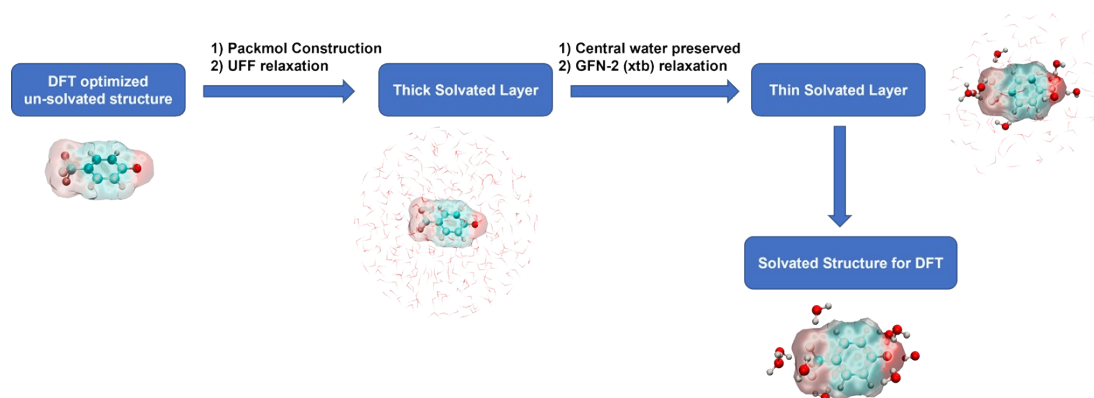


Figure S8. Workflow to add explicit water solvation to RDS-related intermediate and transition state structures.

Table S5. DFT results of the ΔG^\ddagger of 4-TFMP, 2-Cl-4-TFMP, and 2-TFMP spontaneous defluorination based on hybrid solvation model with different number of water molecules. The optimal, DFT pathways with minimum energy barriers are highlighted.

ΔG^\ddagger (kcal/mol)	one H_2O^a	two H_2O^b	five H_2O^c (1)	five H_2O^c (2)	five H_2O^c (3)	six H_2O^d
Compound						
4-TFMP	25.8	26.7	21.2	26.8	21.6	25.0
2-Cl-4-TFMP	28.3	28.2	25.9	31.2	25.4	28.9
2-TFMP	30.7	30.4	24.6	23.9	26.1	22.6

^a in transition state structures, one water molecule explicitly solvates the leaving F^- ;

^b in transition state structures, one water molecule explicitly solvates the phenolate and the other one solvates the leaving F^- ;

^c in transition state structures, two water molecules explicitly solvate the phenolate and the other three solvate the leaving F^- , the orientation of water molecules is different in scenarios (1), (2), or (3);

^d in transition state structures, three water molecules explicitly solvate the phenolate and the other three

solvate the leaving F^- .

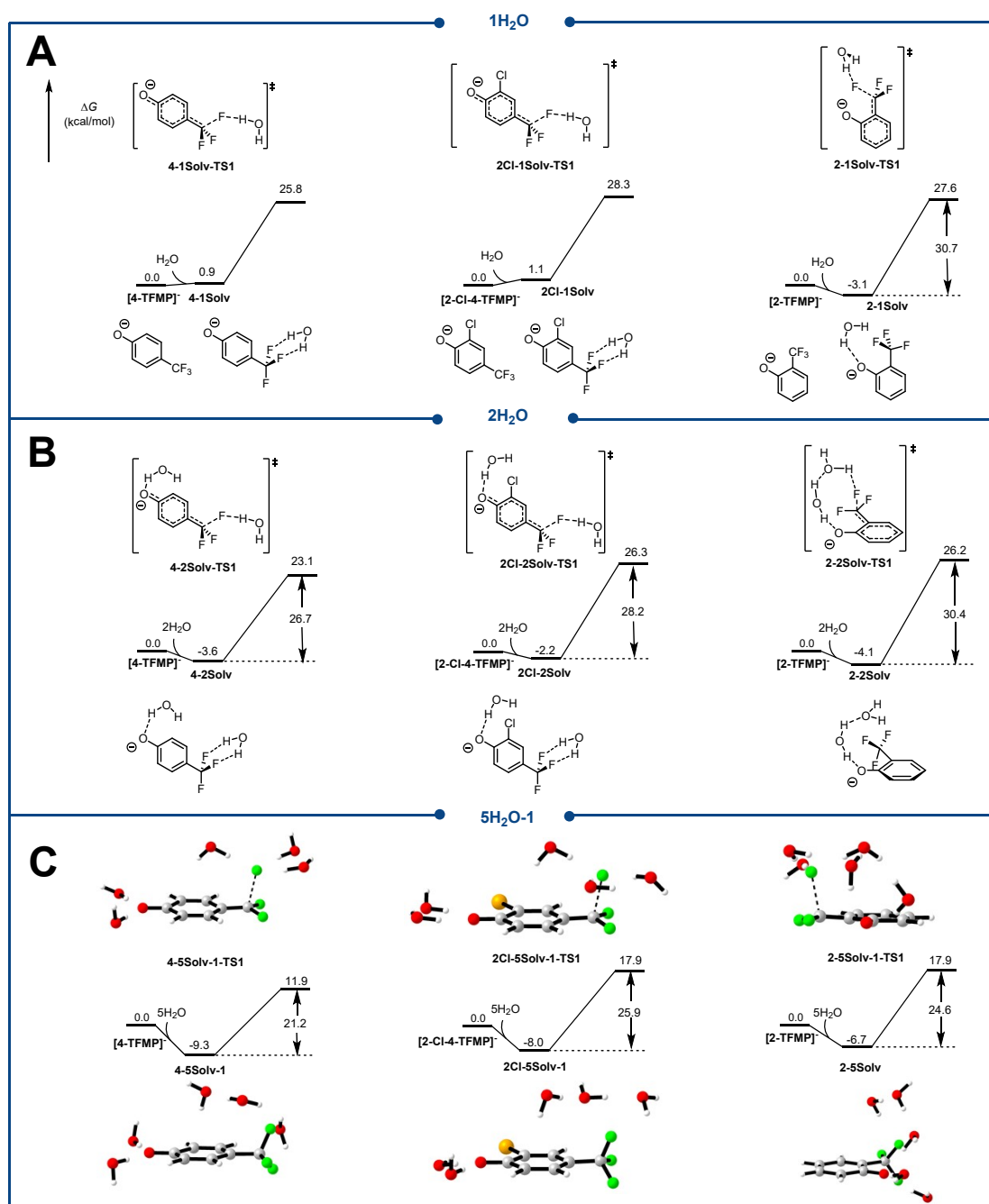


Figure S9. Explicit solvation was applied to calculate the rate determining steps of TFMPs spontaneous defluorination in aqueous phase. Explicit waters in structures are visualization of modeling and may not fully represent the dynamic solvation environment. (A) one water molecule involved; (B) two water molecules involved; (C) five water molecules involved (scenario 1). CYLview was used to visualize the structures.¹³

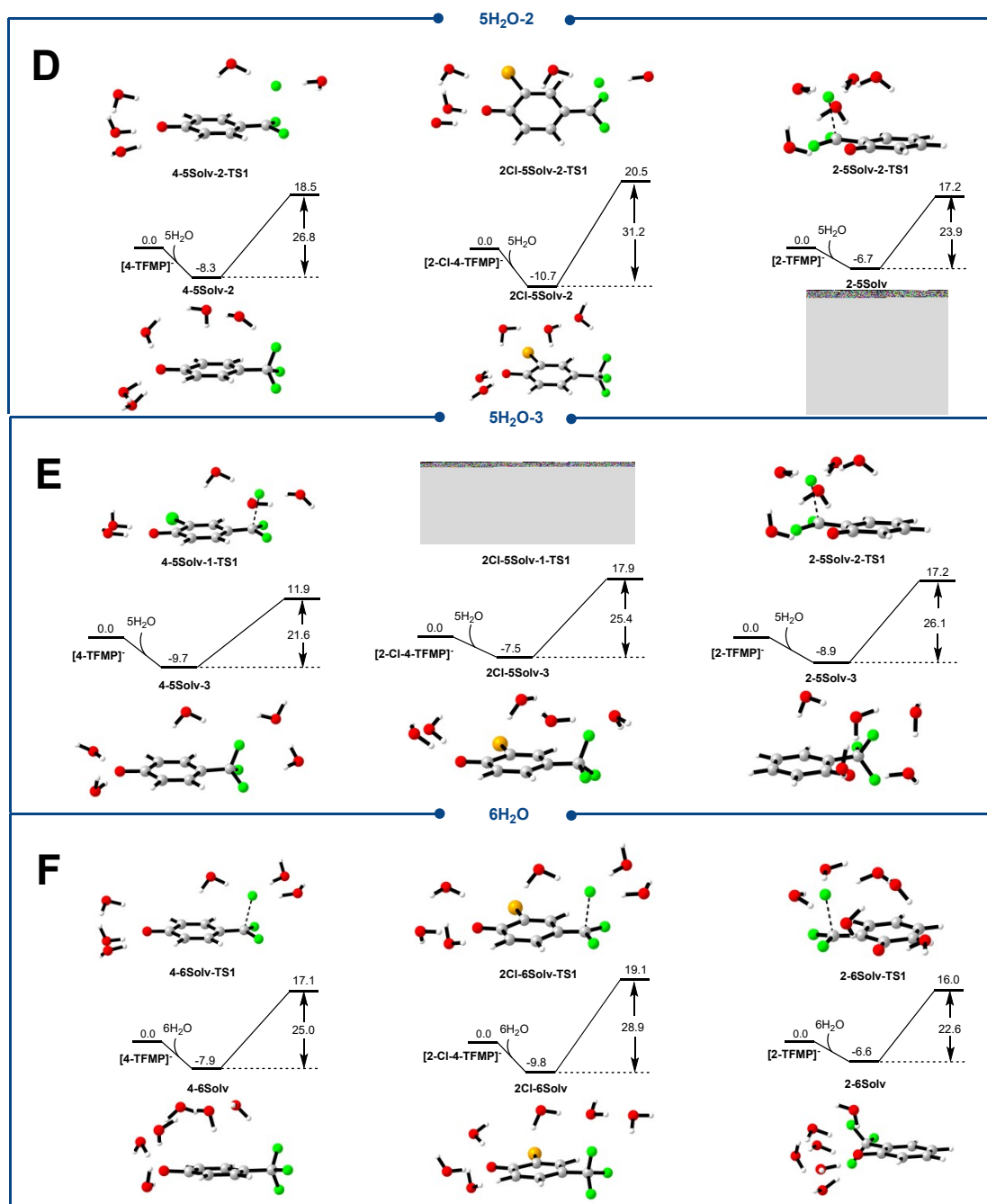


Figure S9 (continued). Explicit solvation was applied to calculate the rate determining steps of TFMPs spontaneous defluorination in aqueous phase. Explicit waters in structures are visualization of modeling and may not fully represent the dynamic solvation environment. (D) five water molecules involved (scenario 2); (E) five water molecules involved (scenario 3); (F) six water molecules involved. CYLview was used to visualize the structures.¹³

SI-12. Pathways Calculated by DFT for 2-Cl-4-TFMP and 2-TFMP Spontaneous Defluorination.

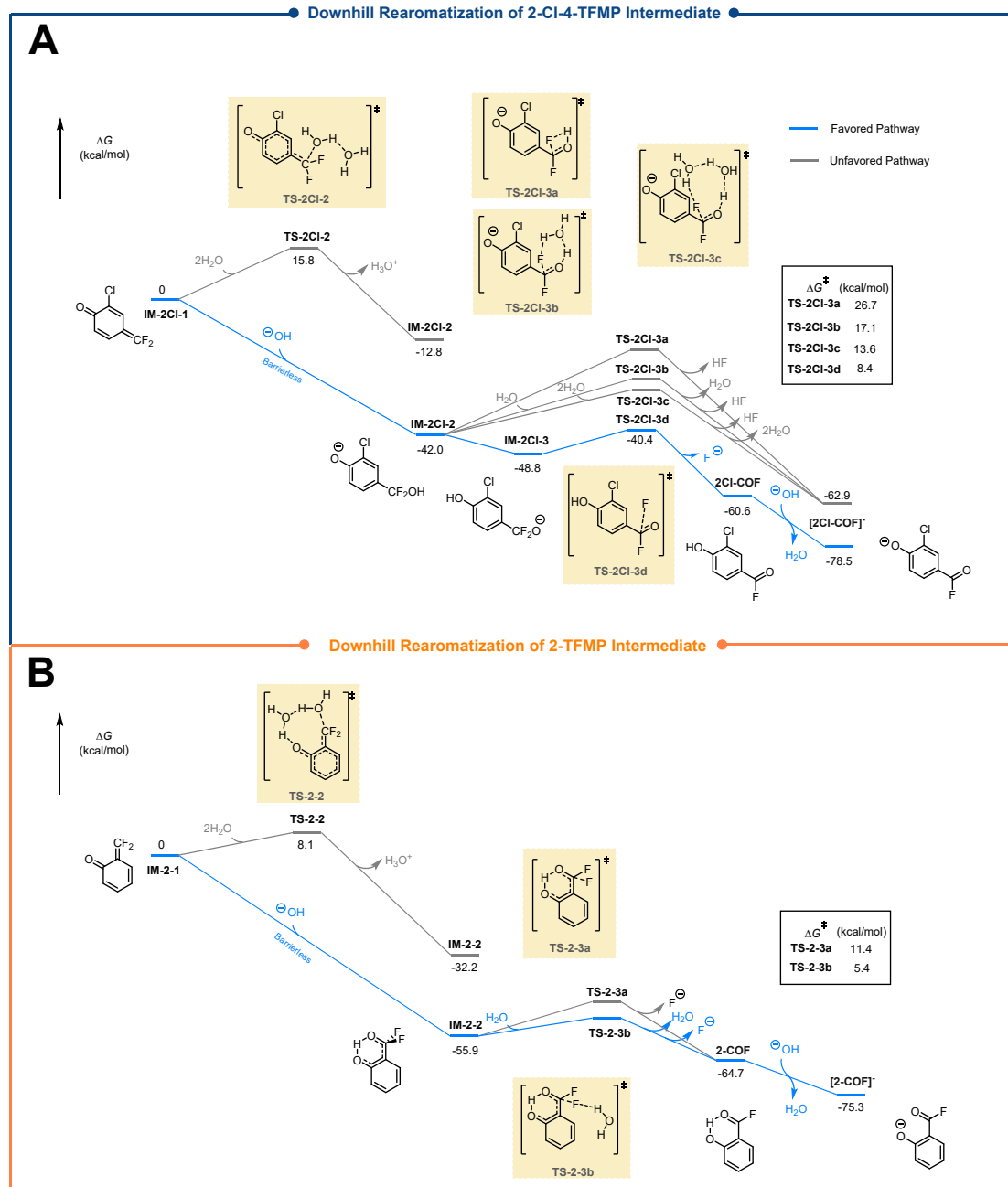


Figure S10. Downhill rearomatization of quinone difluoromethide intermediates for 2-Cl-4-TFMP (A) and 2-TFMP (B).

SI-13. Potential Energy Surface (PES) Scan.

To validate the reaction between difluoromethylene quinone intermediates and OH^- is barrierless, PES was carried out at M06-2X/6-311+g(d,p)/IEFPCM level of theory. In the figure below, the y-axis was the relative electronic energy (ΔEE , kcal/mol), and the x-axis was the scanned C–O distance between the CF_2 carbon and the OH oxygen.

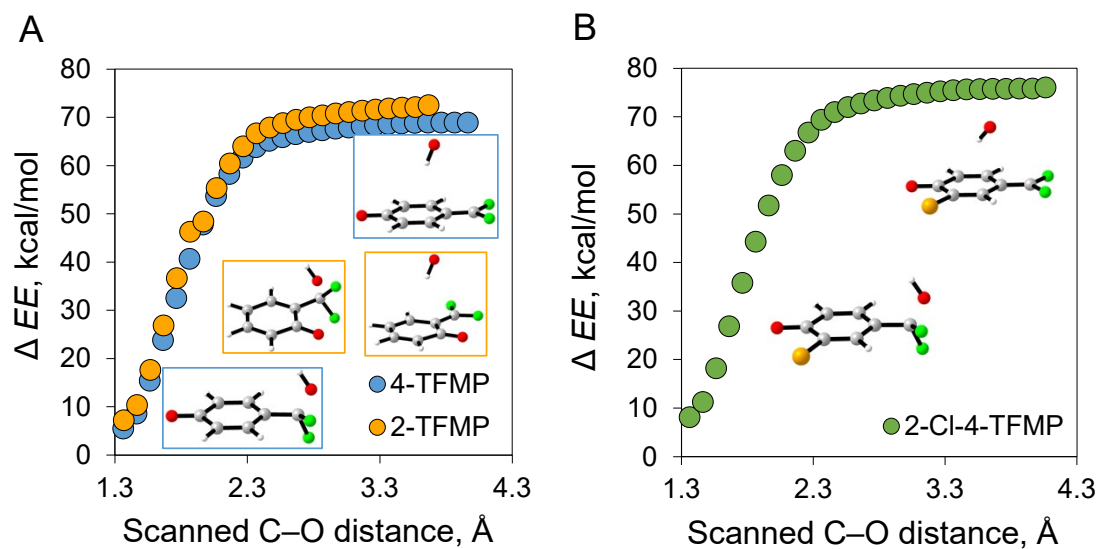


Figure S11. The relative PES scan for the reaction between difluoromethylene quinone intermediates and OH^- . (A) (blue line) the difluoromethylene quinone intermediate generated from 4-TFMP, (orange line) the difluoromethylene quinone intermediate generated from 2-TFMP; (B) the difluoromethylene quinone intermediate generated from 2-Cl-4-TFMP.

References

- 1 J. J. Fifen, Z. Dhaouadi and M. Nsangou, Revision of the Thermodynamics of the Proton in Gas Phase, *J. Phys. Chem. A*, 2014, **118**, 11090–11097.
- 2 J. R. P. Jr and J. M. Riveros, Gibbs energy of solvation of organic ions in aqueous and dimethyl sulfoxide solutions, *Phys. Chem. Chem. Phys.*, 2002, **4**, 1622–1627.
- 3 M. D. Tissandier, K. A. Cowen, W. Y. Feng, E. Gundlach, M. H. Cohen, A. D. Earhart, J. V. Coe and T. R. Tuttle, The Proton's Absolute Aqueous Enthalpy and Gibbs Free Energy of Solvation from Cluster-Ion Solvation Data, *J. Phys. Chem. A*, 1998, **102**, 7787–7794.
- 4 A. V. Marenich, C. J. Cramer and D. G. Truhlar, Universal Solvation Model Based on Solute Electron Density and on a Continuum Model of the Solvent Defined by the Bulk Dielectric Constant and Atomic Surface Tensions, *J. Phys. Chem. B*, 2009, **113**, 6378–6396.
- 5 A. E. Reed, R. B. Weinstock and F. Weinhold, Natural population analysis, *J. Chem. Phys.*, 1985, **83**, 735–746.
- 6 S. P. Ozkorucuklu, J. L. Beltrán, G. Fonrodona, D. Barrón, G. Alsancak and J. Barbosa, Determination of Dissociation Constants of Some Hydroxylated Benzoic and Cinnamic Acids in Water from Mobility and Spectroscopic Data Obtained by CE-DAD, *J. Chem. Eng. Data*, 2009, **54**, 807–811.
- 7 *CRC handbook of chemistry and physics : a ready-reference book of chemical and physical data*, CRC Press, Taylor & Francis Group, 2018th–2019th, 99th edition edn., 2018.
- 8 A. Arcelli and C. Concilio, Polyelectrolyte effects exerted by poly(ethyleneimine) on the ionization constant of substituted phenols, *J. Chem. Soc. Perkin Trans. 2*, 1989, 887–892.
- 9 L. Martínez, R. Andrade, E. G. Birgin and J. M. Martínez, PACKMOL: A package for building initial configurations for molecular dynamics simulations, *J. Comput. Chem.*, 2009, **30**, 2157–2164.
- 10 A. K. Rappe, C. J. Casewit, K. S. Colwell, W. A. I. Goddard and W. M. Skiff, UFF, a full periodic table force field for molecular mechanics and molecular dynamics simulations, *J. Am. Chem. Soc.*, 1992, **114**, 10024–10035.
- 11 C. Bannwarth, S. Ehlert and S. Grimme, GFN2-xTB—An Accurate and Broadly Parametrized Self-Consistent Tight-Binding Quantum Chemical Method with Multipole Electrostatics and Density-Dependent Dispersion Contributions, *J. Chem. Theory Comput.*, 2019, **15**, 1652–1671.
- 12 C. Bannwarth, E. Caldeweyher, S. Ehlert, A. Hansen, P. Pracht, J. Seibert, S. Spicher and S. Grimme, Extended tight-binding quantum chemistry methods, *WIREs Comput. Mol. Sci.*, 2021, **11**, e1493.
- 13 C. Y. Legault, CYLview20, Université de Sherbrooke, 2020 (<http://www.cylview.org>).